1 Benchmark Results

In this supplemental material we provide the results of several well known benchmarks using TerraFERMA. For each case we provide a brief description of the benchmark and the convergence results produced using TerraFERMA as compared to published solutions, where available. When the non-dimensionalization used in the residual differs from that in the literature our results have been rescaled for comparison. Complete and reproducible `tfml` files and meshes for all the benchmarks can be found as a separate git repository at `bitbucket.org:tferma/benchmarks`.

1.1 Incompressible Two-Dimensional Convection: *Blankenbach et al.* (1989)

Blankenbach et al. (1989) described several benchmarks for incompressible convection in a two-dimensional domain of unit height and aspect ratio l. The prognostic variables are velocity, $\boldsymbol{v}$, pressure p, and temperature, T.

For the steady-state cases (1–2) boundary conditions for temperature are $T = 0$ at the top surface, $z = 1$, $T = 1$ at the base, $z = 0$, with insulating (homogeneous Neumann, $\partial_x T = 0$) side-walls. For velocity, free-slip boundary conditions are specified at all boundaries. Simulations are run until a near steady-state is attained where the variation in the fields is less than 10^{-9} in the infinity-norm.

Case 1a–c Isoviscous steady-state cases are defined in a domain with aspect ratio, $l = 1$, with Rayleigh numbers 10^4, 10^5 and 10^6 (Table 1)

Table 1: Results from 2-D, isoviscous square convection benchmark cases (***Blankenbach et al.*, 1989**).

		Nu	v_{rms}	q_1	q_2	T_e	z_e
Case 1a: Ra $= 10^4$	16×16	4.897	42.884	8.062	0.588	0.423	0.233
	32×32	4.887	42.865	8.060	0.589	0.422	0.226
	64×64	4.885	42.865	8.059	0.589	0.422	0.226
	128×128	4.885	42.865	8.059	0.589	0.422	0.225
	256×256	4.884	42.865	8.059	0.589	0.422	0.225
	Benchmark	4.884	42.865	8.059	0.589	0.422	0.225

		Nu	v_{rms}	q_1	q_2	T_e	z_e
Case 1b: Ra $= 10^5$	16×16	10.570	193.493	19.105	0.722	0.431	0.111
	32×32	10.539	193.222	19.081	0.722	0.428	0.114
	64×64	10.535	193.215	19.080	0.723	0.428	0.111
	128×128	10.534	193.215	19.080	0.723	0.428	0.112
	256×256	10.534	193.214	19.079	0.723	0.428	0.112
	Benchmark	10.534	193.214	19.079	0.723	0.428	0.112

		Nu	v_{rms}	q_1	q_2	T_e	z_e
Case 1c: Ra $= 10^6$	16×16	22.107	836.687	46.187	0.896	0.434	0.061
	32×32	21.982	834.024	46.008	0.877	0.432	0.059
	64×64	21.971	833.990	45.972	0.877	0.432	0.058
	128×128	21.972	833.989	45.967	0.877	0.432	0.058
	Benchmark	21.972	833.990	45.964	0.877	0.432	0.058

Case 2a-b Two variable viscosity steady-state cases were run. For case **2a**, viscosity is temperature dependent with

$$\mu = \exp(-bT_i) \tag{1}$$

and $b = \ln(1000)$. For case **2b** the viscosity is also depth-dependent according to the equation:

$$\mu = \exp\left(-bT_i + c(1-z)\right) \tag{2}$$

where $b = \ln(16384)$ and $c = \ln(64)$. Convergence results are given in Table 2 for Ra $= 10^4$, aspect ratio $l = 1$.

Table 2: Results from 2-D, variable viscosity square convection benchmark cases Ra $= 10^4$ (***Blankenbach et al.*, 1989**).

		Nu	v_{rms}	q_1	q_2	q_3	q_4	T_{e_1}	z_{e_1}	T_{e_2}	z_{e_2}
Case 2a: $\eta(T)$	16×16	10.017	464.066	17.452	0.962	28.926	0.549	0.718	0.067	0.819	0.833
	32×32	10.069	479.951	17.533	1.007	26.892	0.498	0.739	0.062	0.832	0.827
	64×64	10.066	480.385	17.531	1.008	26.813	0.497	0.740	0.063	0.832	0.824
	128×128	10.064	480.257	17.528	1.008	26.807	0.498	0.740	0.063	0.832	0.823
	Benchmark	10.066	480.433	17.531	1.009	26.809	0.497	0.741	0.062	0.832	0.824

		Nu	v_{rms}	q_1	q_2	q_3	q_4	T_{e_1}	z_{e_1}	T_{e_2}	z_{e_2}
Case 2b: $\eta(T, z)$	40×16	6.804	169.098	18.544	0.170	13.963	0.628	0.388	0.181	0.570	0.753
	80×32	6.926	171.648	18.484	0.177	14.162	0.618	0.397	0.189	0.576	0.778
	160×64	6.930	171.754	18.485	0.177	14.168	0.618	0.397	0.191	0.576	0.782
	Benchmark	6.930	171.755	18.484	0.177	14.168	0.618	0.397	0.191	0.576	0.784

1.2 Incompressible Laminar Plumes: *Vatteville et al.* (2009)

Vatteville et al. (2009) performed laboratory experiments where a thermal plume was initiated from a circular heater in a square tank of silicone oil at several heater powers. Approximating the domain to be cylindrically symmetric, they demonstrated that the experimental results could be reproduced to great accuracy by finite element modeling in axisymmetric cylindrical geometry.

Using the same cylindrical approximation we examine four cases, at different heater power levels (0.6, 1.0, 1.7 and 3.3 W). Boundary conditions are chosen to mimic those of the laboratory tank: no–slip conditions are specified on the bottom (including the heater) and the external side of the domain, while free–slip and no normal flow conditions are specified at the top and internal side, $r = 0$. For temperature, the external wall and top boundary are kept at room temperature. The bottom boundary is also held at room temperature, except at the heater itself, where we prescribe the measured time–dependent evolution of heater temperature, from the laboratory experiments (this is available along with other model parameters in *Vatteville et al.* (2009)). Homogeneous Neumann conditions are specified on the internal wall. Adaptive time-stepping targets a maximum Courant number of 2.5.

The model incorporates a temperature dependent viscosity law:

$$\mu = \exp\left(b_0 + \frac{b_1}{T_i + \Delta T}\right), \tag{3}$$

Results are presented in the Figure 1. In Figure 1(a), we plot the maximum velocity along the plume conduit, as a function of time, for the experimental data and for fixed and adaptive mesh simulations. The experimentally measured velocity field is slightly noisy, due to the statistical nature of Particle Image Velocimetry (PIV), but compares quantitatively well with the velocity field predicted by TerraFERMA, over a range of supplied powers and, hence, over a range of heater temperatures. We consistently observe that the near–steady plume conduit velocity predicted numerically is higher than the laboratory measurements. Identical discrepancies were observed between the numerical and laboratory results of *Vatteville et al.* (2009).

One critical aspect of the laboratory measurements is that the PIV method uses an averaging window that is necessary to compile statistically meaningful velocities (see *Vatteville et al.*, 2009, for further details).

To mimic the effects of this averaging, we post–process numerical results by averaging in 3 mm squares over the domain. Averaging has the effect of reducing the discrepancy between experimentally sampled and numerically predicted velocities (Figure 1).

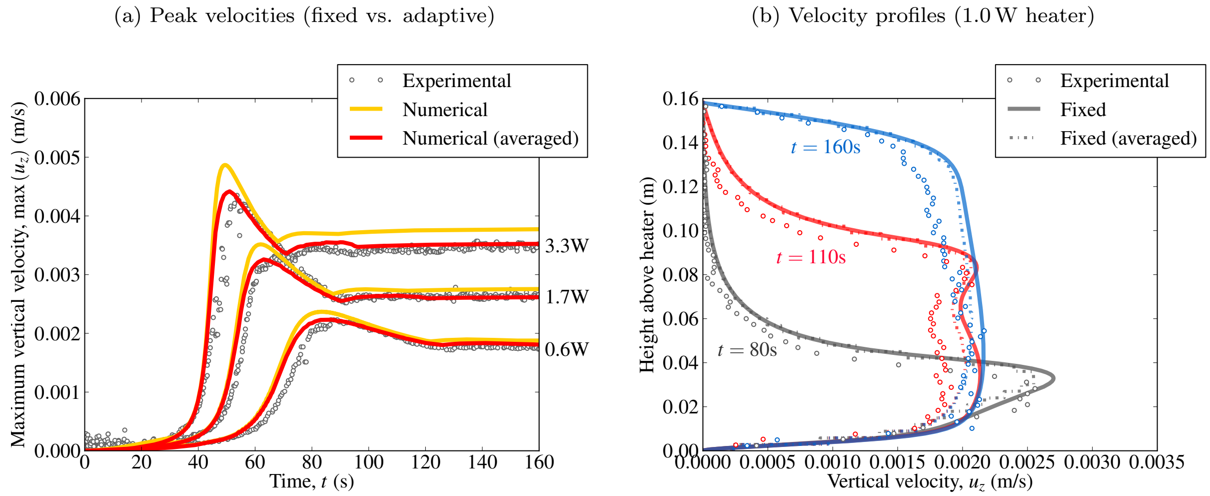

Figure 1: (a) Benchmark results for *Vatteville et al.* (2009) showing maximum velocities vs. time in the laboratory experiments and the numerical simulations for a cylindrical plume. Following *Vatteville et al.* (2009), the numerical data is averaged in 3 mm squares to mimic the effect of laboratory data collection. The effect of this averaging can also be seen in velocity profiles of the numerical and laboratory data above the heater (b, heater power of 1.0 W).

1.3 Compressible Two-Dimensional Convection: *King et al.* (2010)

King et al. (2010) defined a series of convection benchmarks similar to those of *Blankenbach et al.* (1989) but with a linearized compressible equation of state. Solutions are sought for velocity, $\boldsymbol{v}$, and perturbations in the temperature, T, and pressure p, from prescribed reference states, $\bar{T}$ and $\bar{p}$ respectively, corresponding to a reference density $\bar{\rho}$. The importance of compressibility is now indicated by the non-dimensional dissipation number Di. Full details of the derivation can be found in *King et al.* (2010); *Schubert et al.* (2001). A reduced subset of these parameters is considered here for benchmarking purposes. In all cases the domain is a two-dimensional square of unit dimensions with free-slip boundary conditions for the Stokes equtions at all boundaries. The side walls are insulating (homogeneous Neumann, $\partial_x T = 0$) for temperature while $T = 0$ is specified at the top surface.

Extended Boussinesq Approximation (EBA) In the extended Boussinesq approximation the velocity field remains divergence free and only the temperature equation sees the addition of terms that scale with the dissipation number. An additional boundary condition for temperature, $T = 1$ is applied at the base of the domain. Simulations are run at a variety of resolutions, all structured but with refinement at the boundaries. Convergence results for **EBA** and a range of Ra and Di can be found in tables 3–4.

Truncated Anelastic Liquid Approximation (TALA) A first approximation that includes the effects of compressibility in the Stokes equations, but ignoring the pressure effect on buoyancy is the truncated anelastic liquid approximation (TALA). The velocity field now has a non-zero divergence. Since we solve our equations in potential temperature we use a modified temperature condition at the lower boundary, which is now given by $T = 1 + T_0\,(1 - \exp(\mathrm{Di}))$. Simulations are run at a variety of resolutions, all structured but with refinement at the boundaries. Convergence results for **TALA** for a range of Ra, and Di can be found in tables 5–6.

Anelastic Liquid Approximation (ALA) In the anelastic liquid approximation (ALA) the effects of the pressure on buoyancy are now included. As in TALA the temperature at the base of the domain is given by $T = 1 + T_0\,(1 - \exp(\mathrm{Di}))$. Simulations are run at a variety of resolutions, all structured but with refinement at the boundaries. Convergence results for **ALA** for a range of Ra, and Di can be found in tables 7–9.

Temperature Dependent Viscosity ALA One set of benchmarks uses the same temperature-dependence of viscosity as in the *Blankenbach et al.* (1989) case 2a. Simulations are run at a variety of resolutions, all structured but with refinement at the boundaries. Convergence results for a range of Ra, and Di can be found in tables 10

Table 3: Results from 2-D, isoviscous square convection benchmark cases using the extended Bousinesq approximation (**EBA**) at $\mathrm{Ra} = 10^4$ **(*King et al.*, 2010)**

		Nu	v_{rms}	$\max(u\|_{z=1})$	$< u\|_{z=1} >$	$< T + \bar{T} >$	$< \varphi >$	$< W >$
	16×16	4.103	38.469	54.941	36.604	0.491	0.774	0.774
	32×32	4.096	38.455	54.869	36.592	0.491	0.773	0.773
	64×64	4.095	38.455	54.868	36.592	0.491	0.773	0.773
	128×128	4.095	38.455	54.868	36.592	0.491	0.773	0.773
Di = 0.25	Benchmark (UM)	4.090	38.400	54.900	36.600	0.491	0.000	0.000
	Benchmark (KS)	4.092	38.434	54.831	36.568	0.491	0.772	0.772
	Benchmark (CZ)	4.046	38.391	54.779	36.513	0.491	0.769	0.769
	Benchmark (VT)	4.096	38.476	54.897	36.599	0.491	0.773	0.774
	Benchmark (CU)	4.090	38.500	54.900	36.600	0.491	0.774	0.775
	Benchmark (CT)	4.084	38.478	54.899	36.600	0.491	0.732	0.774

		Nu	v_{rms}	$\max(u\|_{z=1})$	$< u\|_{z=1} >$	$< T + \bar{T} >$	$< \varphi >$	$< W >$
	16×16	3.388	33.909	48.122	31.802	0.482	1.189	1.189
	32×32	3.383	33.900	48.066	31.793	0.482	1.189	1.189
	64×64	3.382	33.900	48.065	31.793	0.482	1.189	1.189
	128×128	3.382	33.900	48.065	31.793	0.482	1.188	1.189
Di = 0.5	Benchmark (UM)	3.370	33.900	48.000	31.800	0.482	0.000	0.000
	Benchmark (KS)	3.380	33.879	48.033	31.771	0.482	1.187	1.187
	Benchmark (CZ)	3.335	33.760	47.866	31.646	0.482	1.176	1.177
	Benchmark (VT)	3.383	33.918	48.088	31.799	0.482	1.189	1.189
	Benchmark (CU)	3.380	33.900	48.100	31.800	0.482	1.190	1.190
	Benchmark (CT)	3.364	33.920	48.090	31.800	0.482	1.125	1.189

		Nu	v_{rms}	$\max(u\|_{z=1})$	$< u\|_{z=1} >$	$< T + \bar{T} >$	$< \varphi >$	$< W >$
	16×16	2.196	24.220	34.273	22.241	0.467	1.188	1.188
	32×32	2.194	24.220	34.245	22.238	0.467	1.187	1.187
	64×64	2.194	24.220	34.245	22.238	0.467	1.187	1.187
	128×128	2.194	24.220	34.245	22.238	0.467	1.187	1.187
Di = 1.0	Benchmark (UM)	2.190	24.200	34.200	22.200	0.467	0.000	0.000
	Benchmark (KS)	2.193	24.202	34.219	22.222	0.467	1.185	1.186
	Benchmark (CZ)	2.153	23.950	33.871	21.983	0.466	1.159	1.159
	Benchmark (VT)	2.194	24.232	34.260	22.243	0.467	1.188	1.188
	Benchmark (CU)	2.190	24.200	34.300	22.200	0.467	1.188	1.189
	Benchmark (CT)	2.176	24.237	34.265	22.246	0.467	1.126	1.188

Table 4: Results from 2-D, isoviscous square convection benchmark cases using the extended Bousinesq approximation (**EBA**) at Ra $= 10^5$ (***King et al.*, 2010**)

		Nu	v_{rms}	$\max(u\vert_{z=1})$	$< u\vert_{z=1} >$	$< T+\bar{T} >$	$< \varphi >$	$< W >$
	16×16	8.681	174.126	239.952	175.699	0.505	1.917	1.917
	32×32	8.656	173.905	239.519	175.485	0.505	1.912	1.912
	64×64	8.653	173.901	239.513	175.480	0.505	1.912	1.912
	128×128	8.653	173.901	239.513	175.480	0.505	1.912	1.912
Di $= 0.25$	Benchmark (UM)	8.610	174.000	239.700	175.500	0.504	0.000	0.000
	Benchmark (KS)	8.623	173.480	238.940	175.000	0.504	1.900	1.901
	Benchmark (CZ)	8.540	173.618	239.100	175.199	0.503	1.899	1.901
	Benchmark (VT)	8.655	174.205	239.616	175.537	0.504	1.912	1.912
	Benchmark (CU)	8.630	174.100	239.600	175.500	0.504	1.911	1.914
	Benchmark (CT)	8.629	174.070	239.606	175.537	0.504	1.798	1.912

		Nu	v_{rms}	$\max(u\vert_{z=1})$	$< u\vert_{z=1} >$	$< T+\bar{T} >$	$< \varphi >$	$< W >$
	16×16	6.914	153.117	211.086	151.841	0.502	2.947	2.947
	32×32	6.897	152.957	210.899	151.692	0.502	2.941	2.941
	64×64	6.894	152.956	210.874	151.691	0.502	2.941	2.941
	128×128	6.894	152.957	210.872	151.692	0.502	2.941	2.941
Di $= 0.5$	Benchmark (UM)	6.860	153.000	211.000	151.700	0.502	0.000	0.000
	Benchmark (KS)	6.874	152.510	210.280	151.250	0.501	2.919	2.920
	Benchmark (CZ)	6.787	152.269	209.868	151.041	0.500	2.905	2.909
	Benchmark (VT)	6.895	153.394	210.966	151.738	0.502	2.941	2.941
	Benchmark (CU)	6.880	153.100	210.900	151.700	0.502	2.940	2.944
	Benchmark (CT)	6.855	153.094	210.954	151.739	0.501	2.767	2.941

		Nu	v_{rms}	$\max(u\vert_{z=1})$	$< u\vert_{z=1} >$	$< T+\bar{T} >$	$< \varphi >$	$< W >$
	16×16	3.973	108.116	149.904	103.228	0.482	2.945	2.946
	32×32	3.965	108.046	150.080	103.159	0.482	2.941	2.941
	64×64	3.964	108.048	150.080	103.161	0.482	2.941	2.941
	128×128	3.964	108.047	150.079	103.159	0.482	2.940	2.941
Di $= 1.0$	Benchmark (UM)	3.940	108.100	150.200	103.200	0.482	0.000	0.000
	Benchmark (KS)	3.957	107.650	149.610	102.850	0.482	2.914	2.915
	Benchmark (CZ)	3.892	107.130	148.698	102.379	0.479	2.879	2.882
	Benchmark (VT)	3.965	108.141	150.180	103.203	0.482	2.942	2.943
	Benchmark (CU)	3.960	108.200	150.100	103.200	0.482	2.943	2.947
	Benchmark (CT)	3.928	108.197	150.224	103.248	0.482	2.776	2.945

Table 5: Results from 2-D, isoviscous square convection benchmark cases using the truncated anelastic approximation (**TALA**) at $\mathrm{Ra} = 10^4$ ***(King et al., 2010)***

		Nu	v_{rms}	$\max(u\|_{z=1})$	$< u\|_{z=1} >$	$< T + \bar{T} >$	$< \varphi >$	$< W >$
	16×16	4.435	40.070	58.813	39.311	0.513	0.854	0.851
	32×32	4.426	40.048	58.715	39.291	0.513	0.853	0.850
	64×64	4.425	40.047	58.717	39.291	0.513	0.853	0.850
	128×128	4.425	40.047	58.716	39.291	0.513	0.853	0.850
$\mathrm{Di} = 0.25$	Benchmark (UM)	4.416	40.043	58.710	39.276	0.513	0.850	0.850
	Benchmark (KS)	4.424	40.048	58.711	39.289	0.513	0.853	0.850
	Benchmark (CZ)	4.370	40.220	58.990	39.450	0.512	0.859	0.862
	Benchmark (VT)	4.430	40.200	58.740	39.300	0.513	0.854	0.851
	Benchmark (CU)	4.420	40.100	58.700	39.300	0.513	0.854	0.852
	Benchmark (CT)	4.412	40.075	58.741	39.301	0.513	0.807	0.851

		Nu	v_{rms}	$\max(u\|_{z=1})$	$< u\|_{z=1} >$	$< T + \bar{T} >$	$< \varphi >$	$< W >$
	16×16	2.570	26.003	40.611	26.421	0.509	1.464	1.400
	32×32	2.567	26.004	40.581	26.418	0.509	1.463	1.399
	64×64	2.566	26.004	40.586	26.418	0.509	1.463	1.399
	128×128	2.566	26.004	40.587	26.418	0.509	1.463	1.399
$\mathrm{Di} = 1.0$	Benchmark (UM)	2.556	26.007	40.595	26.416	0.509	1.459	1.396
	Benchmark (KS)	2.568	26.011	40.614	26.436	0.509	1.464	1.400
	Benchmark (CZ)	2.510	25.990	40.480	26.350	0.505	1.455	1.425
	Benchmark (VT)	2.570	26.100	40.600	26.400	0.509	1.465	1.400
	Benchmark (CU)	2.570	26.000	40.600	26.400	0.509	1.465	1.402
	Benchmark (CT)	2.542	26.037	40.630	26.440	0.509	1.387	1.401

		Nu	v_{rms}	$\max(u\|_{z=1})$	$< u\|_{z=1} >$	$< T + \bar{T} >$	$< \varphi >$	$< W >$
	16×16	1.364	10.977	19.424	11.663	0.478	0.481	0.447
	32×32	1.362	11.022	19.538	11.698	0.478	0.479	0.448
	64×64	1.362	11.023	19.543	11.699	0.478	0.479	0.448
	128×128	1.362	11.023	19.543	11.699	0.478	0.479	0.448
$\mathrm{Di} = 1.5$	Benchmark (UM)	1.359	11.027	19.557	11.704	0.478	0.477	0.445
	Benchmark (KS)	1.362	11.004	19.539	11.689	0.478	0.478	0.447
	Benchmark (CZ)	1.349	11.156	19.636	11.828	0.476	0.480	0.454
	Benchmark (VT)	1.362	11.073	19.557	11.710	0.478	0.479	0.448
	Benchmark (CU)	1.360	11.000	19.600	11.700	0.478	0.480	0.449
	Benchmark (CT)	1.353	11.051	19.573	11.721	0.478	0.457	0.449

Table 6: Results from 2-D, isoviscous square convection benchmark cases using the truncated anelastic approximation (**TALA**) at $\mathrm{Ra} = 10^5$ (***King et al.*, 2010**)

		Nu	v_{rms}	$\max(u\|_{z=1})$	$< u\|_{z=1} >$	$< T+\bar{T} >$	$< \varphi >$	$< W >$
	16×16	9.292	178.708	254.955	186.231	0.530	2.066	2.061
	32×32	9.263	178.410	254.482	185.918	0.530	2.059	2.054
	64×64	9.259	178.404	254.470	185.912	0.530	2.059	2.054
	128×128	9.258	178.405	254.472	185.913	0.530	2.059	2.054
Di = 0.25	Benchmark (UM)	9.211	178.560	254.716	185.982	0.530	2.046	2.053
	Benchmark (KS)	9.225	177.990	253.890	285.430	0.530	2.046	2.042
	Benchmark (CZ)	9.130	179.400	255.720	187.100	0.527	2.082	2.090
	Benchmark (VT)	9.260	180.200	254.700	186.000	0.530	2.060	2.055
	Benchmark (CU)	9.230	178.600	254.600	186.000	0.530	2.060	2.057
	Benchmark (CT)	9.233	178.630	254.654	186.019	0.530	1.935	2.055

		Nu	v_{rms}	$\max(u\|_{z=1})$	$< u\|_{z=1} >$	$< T+\bar{T} >$	$< \varphi >$	$< W >$
	16×16	3.964	86.143	143.513	92.603	0.530	2.862	2.789
	32×32	3.923	84.796	141.133	91.061	0.530	2.817	2.752
	64×64	3.921	84.752	141.046	91.008	0.530	2.815	2.751
	128×128	3.920	84.753	141.052	91.010	0.530	2.816	2.751
Di = 1.0	Benchmark (UM)	3.907	85.105	141.607	91.345	0.529	2.802	2.750
	Benchmark (KS)	3.933	84.943	141.470	91.503	0.530	2.791	2.729
	Benchmark (CZ)	3.980	91.060	149.110	98.140	0.521	2.974	2.955
	Benchmark (VT)	3.920	86.080	141.300	91.100	0.530	2.821	2.757
	Benchmark (CU)	3.920	85.100	141.400	91.300	0.530	2.828	2.772
	Benchmark (CT)	3.894	85.150	141.517	91.377	0.529	2.675	2.764

		Nu	v_{rms}	$\max(u\|_{z=1})$	$< u\|_{z=1} >$	$< T+\bar{T} >$	$< \varphi >$	$< W >$
	16×16	2.063	37.011	50.844	0.101	0.462	1.490	1.415
	32×32	2.054	37.384	51.263	0.011	0.461	1.467	1.416
	64×64	2.052	37.389	51.287	0.001	0.461	1.466	1.416
	128×128	2.051	37.389	51.286	0.000	0.461	1.466	1.416
Di = 1.5	Benchmark (UM)	2.041	37.519	51.588	0.357	0.461	1.455	1.422
	Benchmark (KS)	2.053	36.951	51.215	0.000	0.462	1.433	1.386
	Benchmark (CZ)	2.016	37.863	51.238	0.001	0.459	1.469	1.409
	Benchmark (VT)	2.052	38.145	51.353	0.000	0.461	1.473	1.423
	Benchmark (CU)	2.050	37.600	51.400	32.100	0.461	1.476	1.432
	Benchmark (CT)	2.029	37.666	51.417	0.000	0.461	1.406	1.429

Table 7: Results from 2-D, isoviscous square convection benchmark cases using the anelastic liquid approximation (**ALA**) at $\mathrm{Ra} = 10^4$ (***King et al.*, 2010**)

		Nu	v_{rms}	$\max(u\|_{z=1})$	$< u\|_{z=1} >$	$< T+\bar{T} >$	$< \varphi >$	$< W >$
Di = 0.25	16×16	4.425	39.977	58.148	38.841	0.515	0.851	0.850
	32×32	4.417	39.957	58.055	38.823	0.515	0.850	0.849
	64×64	4.415	39.957	58.057	38.822	0.515	0.850	0.849
	128×128	4.415	39.957	58.057	38.822	0.515	0.850	0.849
	Benchmark (UM)	4.406	39.952	58.048	38.808	0.515	0.847	0.849
	Benchmark (VT)	4.414	40.095	58.085	38.837	0.515	0.849	0.849
	Benchmark (CU)	4.410	40.000	58.100	38.800	0.515	0.849	0.850

		Nu	v_{rms}	$\max(u\|_{z=1})$	$< u\|_{z=1} >$	$< T+\bar{T} >$	$< \varphi >$	$< W >$
Di = 1.0	16×16	2.450	24.631	36.749	23.798	0.512	1.348	1.350
	32×32	2.447	24.659	36.756	23.811	0.512	1.347	1.352
	64×64	2.447	24.660	36.758	23.811	0.512	1.347	1.352
	128×128	2.447	24.660	36.759	23.811	0.512	1.347	1.352
	Benchmark (UM)	2.438	24.663	36.767	-23.811	0.512	1.343	1.349
	Benchmark (VT)	2.472	25.016	37.602	24.401	0.510	1.362	1.362
	Benchmark (CU)	2.470	24.900	37.600	24.400	0.510	1.363	1.364

		Nu	v_{rms}	$\max(u\|_{z=1})$	$< u\|_{z=1} >$	$< T+\bar{T} >$	$< \varphi >$	$< W >$
Di = 1.5	16×16	1.293	9.652	16.034	9.551	0.481	0.416	0.388
	32×32	1.288	9.830	16.226	9.678	0.479	0.395	0.398
	64×64	1.287	9.833	16.231	9.679	0.479	0.394	0.398
	128×128	1.287	9.833	16.231	9.679	0.479	0.394	0.398
	Benchmark (UM)	1.285	9.835	16.242	9.683	0.479	0.393	0.396
	Benchmark (VT)	1.311	10.240	17.232	10.302	0.478	0.417	0.417
	Benchmark (CU)	1.310	10.200	17.200	10.300	0.479	0.417	0.417

Table 8: Results from 2-D, isoviscous square convection benchmark cases using the anelastic liquid approximation (**ALA**) at Ra $= 10^5$ ***(King et al., 2010)***

		Nu	v_{rms}	$\max(u\|_{z=1})$	$< u\|_{z=1} >$	$< T+\bar{T} >$	$< \varphi >$	$< W >$
Di = 0.25	16×16	9.274	178.351	252.738	184.570	0.532	2.060	2.059
	32×32	9.246	178.079	252.305	184.273	0.532	2.053	2.052
	64×64	9.242	178.074	252.292	184.267	0.532	2.053	2.052
	128×128	9.242	178.075	252.294	184.268	0.532	2.053	2.052
	Benchmark (UM)	9.196	178.229	252.540	184.336	0.532	2.041	2.051
	Benchmark (VT)	9.243	179.752	252.459	184.371	0.532	2.052	2.052
	Benchmark (CU)	9.210	178.200	252.400	184.300	0.532	2.050	2.054

		Nu	v_{rms}	$\max(u\|_{z=1})$	$< u\|_{z=1} >$	$< T+\bar{T} >$	$< \varphi >$	$< W >$
Di = 1.0	16×16	3.903	85.017	138.074	89.345	0.530	2.817	2.787
	32×32	3.872	84.282	136.478	88.305	0.530	2.757	2.765
	64×64	3.869	84.252	136.393	88.263	0.530	2.756	2.764
	128×128	3.869	84.254	136.402	88.265	0.530	2.756	2.764
	Benchmark (UM)	3.857	84.587	136.877	-88.567	0.530	2.742	2.765
	Benchmark (VT)	3.878	85.580	137.166	88.787	0.529	2.761	2.761
	Benchmark (CU)	3.880	84.600	137.200	88.800	0.529	2.765	2.774

		Nu	v_{rms}	$\max(u\|_{z=1})$	$< u\|_{z=1} >$	$< T+\bar{T} >$	$< \varphi >$	$< W >$
Di = 1.5	16×16	2.029	34.463	48.817	-1.890	0.468	1.592	1.333
	32×32	1.985	36.004	47.536	-0.016	0.461	1.377	1.400
	64×64	1.983	36.029	47.555	0.001	0.461	1.373	1.401
	128×128	1.982	36.029	47.554	0.000	0.461	1.373	1.401
	Benchmark (UM)	1.973	36.141	47.779	0.290	0.461	1.362	1.406
	Benchmark (VT)	1.997	37.130	48.302	0.000	0.461	1.398	1.399
	Benchmark (CU)	2.000	36.600	48.300	30.200	0.461	1.401	1.408

		Nu	v_{rms}	$\max(u\|_{z=1})$	$< u\|_{z=1} >$	$< T+\bar{T} >$	$< \varphi >$	$< W >$
Di = 0.25	16×16	14.855	463.723	658.618	-495.189	0.545	3.447	3.443
	32×32	14.748	462.496	656.357	-493.941	0.545	3.427	3.426
	64×64	14.742	462.490	656.396	-493.931	0.545	3.427	3.425
	128×128	14.743	462.549	656.471	-493.989	0.545	3.428	3.426
	Benchmark (UM)	14.577	462.878	657.024	493.879	0.544	3.391	3.425
	Benchmark (VT)	14.765	469.319	657.594	494.481	0.544	3.434	3.434
	Benchmark (CU)	14.630	463.700	657.700	494.600	0.544	3.427	3.440

Table 9: Results from 2-D, isoviscous square convection benchmark cases using the anelastic approximation **(ALA)** at Ra $= 5 \times 10^5$ **(*King et al.*, 2010)**.

Table 10: Results from 2-D square convection benchmark cases with temperature-dependent rheology using the anelastic liquid approximation (T **dependent ALA**) at $\mathrm{Ra} = 10^4$ (***King et al.*, 2010**)

		Nu	v_{rms}	$\max(u\|_{z=1})$	$< u\|_{z=1} >$	$< T + \bar{T} >$	$< \varphi >$	$< W >$
Di = 0.25	16×16	7.745	355.153	121.870	83.325	0.701	1.739	1.737
	32×32	7.697	352.851	119.174	81.539	0.703	1.637	1.638
	64×64	7.695	353.228	119.137	81.514	0.703	1.635	1.636
	128×128	7.685	351.156	118.900	81.358	0.703	1.631	1.633
	Benchmark (UM)	7.670	370.057	118.106	80.746	0.707	1.636	1.633
	Benchmark (VT)	7.710	381.690	118.600	81.090	0.707	1.644	1.647
	Benchmark (CU)	7.680	371.700	118.500	81.000	0.706	1.643	1.650

		Nu	v_{rms}	$\max(u\|_{z=1})$	$< u\|_{z=1} >$	$< T + \bar{T} >$	$< \varphi >$	$< W >$
Di = 1.0	16×16	2.494	72.500	38.331	24.734	0.558	1.461	1.341
	32×32	2.558	76.471	41.079	26.765	0.554	1.357	1.402
	64×64	2.558	76.490	41.094	26.781	0.554	1.355	1.402
	128×128	2.559	76.545	41.124	26.803	0.554	1.356	1.404
	256×256	2.563	76.773	41.248	26.894	0.553	1.360	1.408
	Benchmark (UM)	2.476	90.879	38.398	24.829	0.557	1.300	1.330
	Benchmark (VT)	2.520	96.790	39.460	25.560	0.557	1.352	1.358
	Benchmark (CU)	2.390	89.500	16.800	10.700	0.556	1.257	1.267

1.4 Idealized Kinematic Subduction Zones: *van Keken et al.* (2008)

van Keken et al. (2008) defines a series of benchmarks for subduction zone thermal structure using a kinematic slab and dynamic wedge. In the simplest case (1a) of isoviscous rheology the velocity can be described analytically and only the heat equation needs to be solved. Subsequent cases explore the solution of the Stokes equations for isoviscous flow (cases 1b and 1c) and the effects of temperature-dependent (case 2a) an temperature- and stress-dependent rheology (case 2b).

Convergence results for cases 1a–c are in Table 11.

Table 11: Results from 2-D, **kinematic subduction model (*van Keken et al.*, 2008)**

		$T_{60,-60}$	$\lVert T\rVert_2$ Slab	$\lVert T\rVert_2$ Wedge
Case 1a: analytic corner flow	4.00	386.59	503.17	854.04
	2.00	387.76	503.60	854.37
	1.00	388.18	503.76	854.51
	0.50	388.31	503.80	854.54
	0.25	388.35	503.82	854.54
	Benchmark (UM)	388.24	503.77	852.89
	Benchmark (PGC)	388.21	503.69	854.34
	Benchmark (WHOI)	388.26	503.75	854.37

		$T_{60,-60}$	$\lVert T\rVert_2$ Slab	$\lVert T\rVert_2$ Wedge
Case 1b: isoviscous wedge, prescribed BCs	4.00	389.55	504.05	854.21
	2.00	388.50	503.83	854.43
	1.00	388.40	503.83	854.53
	0.50	388.37	503.81	854.53
	Benchmark (UM)	388.22	503.65	854.12
	Benchmark (PGC)	388.21	503.69	854.34
	Benchmark (WHOI)	389.08	504.50	856.08

		$T_{60,-60}$	$\lVert T\rVert_2$ Slab	$\lVert T\rVert_2$ Wedge
Case 1c: isoviscous wedge, free stress BCs	4.00	389.35	503.75	853.50
	2.00	388.10	503.29	853.20
	1.00	387.96	503.24	853.17
	0.50	387.92	503.22	853.16
	Benchmark (UM)	387.84	503.13	852.92
	Benchmark (PGC)	387.78	503.10	852.97
	Benchmark (WHOI)	388.73	504.03	854.99

Convergence results for cases 2a–b are in Table 12

Table 12: Results from 2-D, **kinematic subduction model (*van Keken et al.*, 2008)**

		$T_{60,-60}$	$\|\|T\|\|_2$ Slab	$\|\|T\|\|_2$ Wedge
Case 2a: wedge $\eta(T)$	4.00	576.69	604.81	1001.79
	2.00	580.68	606.95	1003.28
	1.00	580.96	607.13	1003.10
	Benchmark (UM)	580.66	607.11	1003.20
	Benchmark (PGC)	580.52	606.94	1002.85
	Benchmark (WHOI)	581.30	607.26	1003.35

		$T_{60,-60}$	$\|\|T\|\|_2$ Slab	$\|\|T\|\|_2$ Wedge
Case 2b: wedge $\eta(T, \dot{\epsilon})$	4.00	577.28	602.76	998.15
	2.00	583.25	605.01	999.97
	1.00	583.51	605.22	999.97
	Benchmark (UM)	583.36	605.11	1000.01
	Benchmark (PGC)	582.65	604.51	998.71
	Benchmark (WHOI)	583.11	604.96	1000.05

1.5 Linearized Free Surface Flows: *Kramer et al.* (2012)

A set of benchmarks to explore efficient implicit methods for Stokes flow with free surfaces is provided in *Kramer et al.* (2012). The use of a free surface is challenging for many codes due to the short relaxation time of topography in mantle convection settings. Three different cases are presented for an aspect ratio 1 geometry and reflective side boundary conditions. The first cases models the relaxation of the topography on a free surface only at the top of the model. The second provides a free surface also at the base of the model (simulation the core-mantle boundary). The third case is similar to the second one except that a buoyancy force due to a prescribed density anomaly is included as in (*Zhong et al.*, 1996). Convergence results for three general cases are given in Tables 13–15

Table 13: Error between the numerical, η, and analytical, η^*, **free surface elevations** versus time-step size, Δt (***Kramer et al.*, 2012**)

	.	$\|\|(\|\|\eta\|_{z=0}(x) - \eta^*(x)\|\|_2)(t)\|\|_2/D$		$\|\|(\|\|\eta\|_{z=0}(x) - \eta^*\|_{z=0}(x)\|\|_\infty)(t)\|\|_\infty/D$	
	$\Delta t/\tau$	Error	Order	Error	Order
	32.0	1.568e-03		2.941e-04	
	16.0	1.085e-03	0.531	2.593e-04	0.182
	8.0	4.999e-04	1.118	2.001e-04	0.374
1 free surface	4.0	1.747e-04	1.517	1.172e-04	0.771
	2.0	4.551e-05	1.941	4.512e-05	1.377
	1.0	1.050e-05	2.116	1.152e-05	1.970
	0.5	2.505e-06	2.067	2.629e-06	2.131
	0.25	6.175e-07	2.021	6.454e-07	2.026
	0.125	1.541e-07	2.003	1.619e-07	1.995

	.	$\|\|(\|\|\eta\|_{z=0}(x) - \eta^*\|_{z=0}(x)\|\|_2)(t)\|\|_2/D$		$\|\|(\|\|\eta\|_{z=0}(x) - \eta^*\|_{z=0}(x)\|\|_\infty)(t)\|\|_\infty/D$	
	$\Delta t/\tau_-$	Error	Order	Error	Order
	32.0	1.568e-03		2.941e-04	
	16.0	1.085e-03	0.531	2.593e-04	0.182
	8.0	4.999e-04	1.118	2.001e-04	0.374
2 free surfaces top	4.0	1.747e-04	1.517	1.172e-04	0.772
	2.0	4.551e-05	1.941	4.511e-05	1.378
	1.0	1.050e-05	2.116	1.152e-05	1.970
	0.5	2.504e-06	2.068	2.628e-06	2.132
	0.25	6.167e-07	2.022	6.448e-07	2.027
	0.125	1.536e-07	2.006	1.617e-07	1.995

	.	$\|\|(\|\|\eta\|_{z=-D}(x) - \eta^*\|_{z=-D}(x)\|\|_2)(t)\|\|_2/D$		$\|\|(\|\|\eta\|_{z=-D}(x) - \eta^*\|_{z=-D}(x)\|\|_\infty)(t)\|\|_\infty/D$	
	$\Delta t/\tau_-$	Error	Order	Error	Order
	32.0	1.568e-03		2.941e-04	
	16.0	1.085e-03	0.531	2.593e-04	0.182
	8.0	4.999e-04	1.118	2.001e-04	0.374
2 free surfaces bottom	4.0	1.747e-04	1.517	1.172e-04	0.772
	2.0	4.551e-05	1.941	4.512e-05	1.378
	1.0	1.050e-05	2.116	1.152e-05	1.970
	0.5	2.505e-06	2.068	2.628e-06	2.132
	0.25	6.167e-07	2.022	6.445e-07	2.028
	0.125	1.536e-07	2.006	1.615e-07	1.997

Table 14: Error between the numerical, η, and analytical, η^*, **free surface elevations** versus time-step size, Δt for two free surfaces and a density anomaly at depth d (***Kramer et al.*, 2012**)

$z = 0,\ d = D/2$

. $\Delta t/\tau_-$	$\|\|(\|\|\eta\|_{z=0}(x) - \eta^*\|_{z=0}(x)\|\|_2)(t)\|\|_2/D$ Error	Order	$\|\|(\|\|\eta\|_{z=0}(x) - \eta^*\|_{z=0}(x)\|\|_\infty)(t)\|\|_\infty/D$ Error	Order
32.0	1.677e-05		3.146e-06	
16.0	1.161e-05	0.531	2.774e-06	0.182
8.0	5.346e-06	1.118	2.142e-06	0.373
4.0	1.869e-06	1.516	1.256e-06	0.770
2.0	4.874e-07	1.939	4.848e-07	1.374
1.0	1.129e-07	2.110	1.243e-07	1.964
0.5	2.737e-08	2.044	2.846e-08	2.127
0.25	7.609e-09	1.847	7.315e-09	1.960

$z = -D,\ d = D/2$

. $\Delta t/\tau_-$	$\|\|(\|\|\eta\|_{z=-D}(x) - \eta^*\|_{z=-D}(x)\|\|_2)(t)\|\|_2/D$ Error	Order	$\|\|(\|\|\eta\|_{z=-D}(x) - \eta^*\|_{z=-D}(x)\|\|_\infty)(t)\|\|_\infty/D$ Error	Order
32.0	1.677e-05		3.146e-06	
16.0	1.160e-05	0.531	2.774e-06	0.182
8.0	5.345e-06	1.118	2.142e-06	0.373
4.0	1.869e-06	1.516	1.257e-06	0.770
2.0	4.874e-07	1.939	4.849e-07	1.374
1.0	1.129e-07	2.110	1.242e-07	1.965
0.5	2.741e-08	2.042	2.849e-08	2.124
0.25	7.577e-09	1.855	7.244e-09	1.976

$z = 0,\ d = D/4$

. $\Delta t/\tau_-$	$\|\|(\|\|\eta\|_{z=0}(x) - \eta^*\|_{z=0}(x)\|\|_2)(t)\|\|_2/D$ Error	Order	$\|\|(\|\|\eta\|_{z=0}(x) - \eta^*\|_{z=0}(x)\|\|_\infty)(t)\|\|_\infty/D$ Error	Order
32.0	5.006e-05		9.400e-06	
16.0	3.438e-05	0.542	8.260e-06	0.187
8.0	1.570e-05	1.130	6.332e-06	0.383
4.0	5.435e-06	1.531	3.662e-06	0.790
2.0	1.405e-06	1.951	1.389e-06	1.398
1.0	3.253e-07	2.111	3.514e-07	1.983
0.5	7.896e-08	2.043	8.104e-08	2.117
0.25	2.078e-08	1.926	2.040e-08	1.990

$z = -D,\ d = D/4$

. $\Delta t/\tau_-$	$\|\|(\|\|\eta\|_{z=-D}(x) - \eta^*\|_{z=-D}(x)\|\|_2)(t)\|\|_2/D$ Error	Order	$\|\|(\|\|\eta\|_{z=-D}(x) - \eta^*\|_{z=-D}(x)\|\|_\infty)(t)\|\|_\infty/D$ Error	Order
32.0	4.737e-06		8.754e-07	
16.0	3.547e-06	0.417	7.989e-07	0.132
8.0	1.775e-06	0.999	6.610e-07	0.273
4.0	6.755e-07	1.393	4.355e-07	0.602
2.0	1.885e-07	1.841	1.894e-07	1.201
1.0	4.382e-08	2.105	5.289e-08	1.840
0.5	1.054e-08	2.056	1.179e-08	2.166
0.25	3.141e-09	1.746	2.983e-09	1.983

Table 15: Error between the numerical, η, and analytical, η^*, **free surface elevations** versus **grid-size** for two free surfaces and a density anomaly at depth d (***Kramer et al.*, 2012**)

		$\|\|\eta\|_{z=0}(x,t\to\infty)-\eta^*\|_{z=0}(x,t\to\infty)\|\|_2/D$		$\|\|\eta\|_{z=0}(x,t\to\infty)-\eta^*\|_{z=0}(x,t\to\infty)\|\|_\infty$	
		Error	Order	Error	Order
$z=0$, $d=D/2$	20×20	2.061e-08		3.301e-08	
	40×40	5.174e-09	1.994	8.230e-09	2.004
	80×80	1.295e-09	1.999	2.053e-09	2.003
	160×160	3.237e-10	2.000	5.042e-10	2.026
	320×320	8.331e-11	1.958	1.443e-10	1.805

		$\|\|\eta\|_{z=-D}(x,t\to\infty)-\eta^*\|_{z=-D}(x,t\to\infty)\|\|_2/D$		$\|\|\eta\|_{z=-D}(x,t\to\infty)-\eta^*\|_{z=-D}(x,t$	
		Error	Order	Error	Order
$z=-D$, $d=D/2$	20×20	2.061e-08		3.301e-08	
	40×40	5.174e-09	1.994	8.254e-09	2.000
	80×80	1.295e-09	1.999	2.058e-09	2.003
	160×160	3.237e-10	2.000	5.107e-10	2.011
	320×320	8.331e-11	1.958	1.344e-10	1.926

		$\|\|\eta\|_{z=0}(x,t\to\infty)-\eta^*\|_{z=0}(x,t\to\infty)\|\|_2/D$		$\|\|\eta\|_{z=0}(x,t\to\infty)-\eta^*\|_{z=0}(x,t\to\infty)\|\|_\infty$	
		Error	Order	Error	Order
$z=0$, $d=D/4$	20×20	6.268e-08		9.737e-08	
	40×40	1.555e-08	2.011	2.210e-08	2.139
	80×80	3.885e-09	2.001	5.542e-09	1.996
	160×160	9.710e-10	2.000	1.389e-09	1.997
	320×320	2.430e-10	1.999	3.578e-10	1.956

		$\|\|\eta\|_{z=-D}(x,t\to\infty)-\eta^*\|_{z=-D}(x,t\to\infty)\|\|_2/D$		$\|\|\eta\|_{z=-D}(x,t\to\infty)-\eta^*\|_{z=-D}(x,t$	
		Error	Order	Error	Order
$z=-D$, $d=D/4$	20×20	5.511e-09		9.024e-09	
	40×40	1.389e-09	1.988	2.304e-09	1.969
	80×80	3.480e-10	1.997	5.670e-10	2.023
	160×160	8.706e-11	1.999	1.394e-10	2.024
	320×320	2.454e-11	1.827	4.213e-11	1.726

1.6 Magmatic Solitary Wave Benchmarks: *Simpson and Spiegelman* (2011)

Solution of magmatic solitary waves in 2 and 3-D are compared to spectrally accurate sinc-collocation solutions given in *Simpson and Spiegelman* (2011). These problems solve a completely different set of coupled equations from thermal convection for porosity φ and "compaction pressure" $\mathcal{P}$

$$\frac{\partial\varphi}{\partial t} + \boldsymbol{v}\cdot\nabla\varphi = \left(\frac{h}{\delta}\right)^2 \varphi^m \mathcal{P} \tag{4}$$

$$-\nabla\cdot\varphi^n\nabla\mathcal{P} + \left(\frac{h}{\delta}\right)^2 \varphi^m\mathcal{P} = \nabla\cdot\varphi^n\boldsymbol{k} \tag{5}$$

(see Figure 2). These benchmarks are particularly nice in that they are a fully non-linear solution that propagates at constant speed c (which depends on wave amplitude) without changing shape. Any errors in shape or propagation velocity can be directly attributed to numerical error. In particular, in a moving frame with velocity $\boldsymbol{v} = -c$, the waves should appear to stand still.

These benchmarks are also a good test of advanced advection schemes for hyperbolic problems and we currently have benchmarks for standard CG advection without stabilization and semi-Lagrangian advection schemes. Figure 2 shows errors in shape and velocity as a function of mesh and time step refinement for a 2-D wave propagating at speed $c = 5$ and permeability exponent $n = 3$ and porosity independent bulk viscosity $m = 0$ using a semi-Lagrangian advection scheme. Tables 1.6–1.6 show results for additional 2 and 3-D waves. For each table N is the number of square cells in each direction (with right/left diagonals for division into triangles), $c\Delta t/\delta$ is the number of compaction lengths (at the background porosity) that a solitary wave travels in one timestep,

$$||e_\varphi|| = \min_\lambda \frac{\sqrt{\int_\Omega(\varphi_{exact} - \varphi_h(\boldsymbol{x}-\boldsymbol{\lambda}))^2\,dx}}{\sqrt{\int_\Omega(\varphi_{exact})^2\,dx}}$$

is the L2 norm of the relative shape error for the numerical wave φ_h that is translated by phase error $\boldsymbol{\lambda}$ to minimize the misfit between the numerical solution and the exact solitary wave (see *Simpson and Spiegelman*, 2011, for detials of error analysis). $||e_c|| = |1 - c/c_{exact}|$ is the relative velocity error.

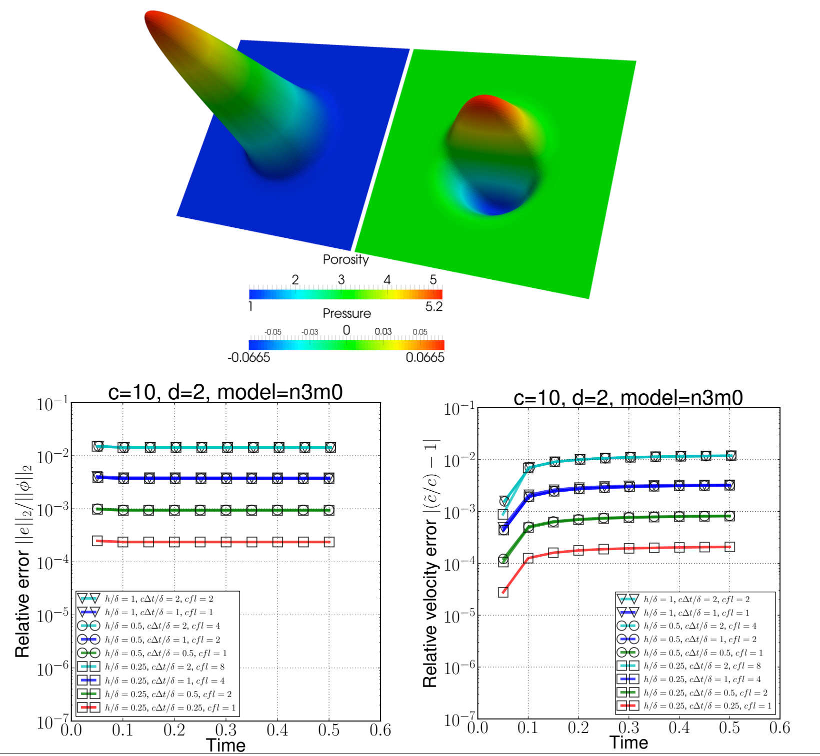

Figure 2: Example magmatic solitary wave benchmarks from *Simpson and Spiegelman* (2011). Top figure shows porosity and pressure fields for a 2D porosity wave with speed $c = 10$, permeability exponent $n = 3$, and bulk-viscosity exponent $m = 0$. These waves should propagate at constant porosity c without changing form and provides a fully non-linear benchmark problem. Lower figures show shape and velocity errors as a function of time . This benchmark solves the problem in a frame moving with the solitary waves using a semi-Lagrangian advection scheme in TerraFERMA. Additional results for other amplitude waves in 2D and 3D, and other advection schemes are in Appendix 1.6.

Table 16: **2-D Solitary Wave Benchmarks (*Simpson and Spiegelman*, 2011)**, phase and velocity errors as a function of grid-spacing and time step for waves with different parameters and background advection schemes, domain height $h = 64\delta$ compaction lengths.

	N	$c\Delta t/\delta$	$\|\|\epsilon_\varphi\|\|$	$\|\|\epsilon_c\|\|$
$c = 10, n = 3, m = 0$, semi-Lagrangian	32×32	2.00	1.427786e-02	1.182138e-02
	32×32	1.00	3.819159e-03	3.255477e-03
	32×32	0.50	1.634865e-03	8.485232e-04
	32×32	0.25	2.202831e-03	3.357135e-04
	64×64	2.00	1.424202e-02	1.188175e-02
	64×64	1.00	3.690917e-03	3.187174e-03
	64×64	0.50	9.481209e-04	8.235713e-04
	64×64	0.25	4.243532e-04	1.921914e-04
	128×128	2.00	1.424087e-02	1.188190e-02
	128×128	1.00	3.686779e-03	3.194658e-03
	128×128	0.50	9.306871e-04	8.119311e-04
	128×128	0.25	2.365556e-04	2.073026e-04

	N	$c\Delta t/\delta$	$\|\|\epsilon_\varphi\|\|$	$\|\|\epsilon_c\|\|$
$c = 10, n = 3, m = 0$, CG	32×32	2.00	8.835990e-04	2.709490e-04
	32×32	1.00	7.604301e-04	2.312489e-04
	32×32	0.50	7.371377e-04	2.097575e-04
	32×32	0.25	7.323057e-04	1.985828e-04
	64×64	2.00	1.741160e-04	2.610058e-05
	64×64	1.00	1.681647e-04	2.055717e-05
	64×64	0.50	1.672073e-04	1.762228e-05
	64×64	0.25	1.670081e-04	1.612605e-05
	128×128	2.00	2.428449e-06	2.930989e-14
	128×128	1.00	4.117082e-05	4.633838e-06
	128×128	0.50	4.098354e-05	3.954427e-06
	128×128	0.25	4.094902e-05	3.607756e-06

	N	$c\Delta t/\delta$	$\|\|\epsilon_\varphi\|\|$	$\|\|\epsilon_c\|\|$
$c = 4, n = 2, m = 1$, semi-Lagrangian	32×32	1.00	1.915212e-02	2.256723e-02
	32×32	0.50	6.714826e-03	5.776035e-03
	32×32	0.25	4.611508e-02	8.089975e-03
	64×64	1.00	1.876294e-02	2.119909e-02
	64×64	0.50	4.795988e-03	5.561606e-03
	64×64	0.25	2.089005e-03	1.366693e-03
	128×128	1.00	1.875865e-02	2.119084e-02
	128×128	0.50	4.688778e-03	5.376917e-03
	128×128	0.25	1.194047e-03	1.380713e-03

	N	$c\Delta t/\delta$	$\|\|\epsilon_\varphi\|\|$	$\|\|\epsilon_c\|\|$
$c = 4, n = 2, m = 1$, CG	32×32	1.00	4.823322e-02	-4.531919e-04
	32×32	0.50	4.458121e-02	-3.441524e-04
	32×32	0.25	5.918820e-02	-6.326548e-04
	64×64	1.00	3.482794e-02	1.385123e-04
	64×64	0.50	2.999372e-02	2.178347e-05
	64×64	0.25	1.654382e-02	-1.248202e-05
	128×128	1.00	1.084181e-02	8.233406e-05
	128×128	0.50	1.399268e-02	8.142084e-05
	128×128	0.25	3.973455e-04	1.237014e-06

Table 17: **3-D Solitary Wave Benchmarks (*Simpson and Spiegelman*, 2011)**, phase and velocity errors as a function of grid-spacing and time step, CG advection, $c = 5$, $n = 3$, $m = 0$ waves

	N	$c\Delta t/\delta$	$\lvert\lvert\epsilon_\varphi\rvert\rvert$	$\lvert\lvert\epsilon_c\rvert\rvert$
	16×16×16	0.50	7.654854e-03	-3.820873e-03
$h/\delta = 64$	16×16×16	0.25	7.799173e-03	-3.676605e-03
	32×32×32	0.50	1.247889e-03	-3.026720e-04
	32×32×32	0.25	1.259622e-03	-2.908826e-04

	N	$c\Delta t/\delta$	$\lvert\lvert\epsilon_\varphi\rvert\rvert$	$\lvert\lvert\epsilon_c\rvert\rvert$
	16×16×16	1.00	2.264073e-03	-1.264844e-03
$h/\delta = 32$ (higher resolution)	16×16×16	0.50	2.289875e-03	-1.251693e-03
	32×32×32	1.00	1.184534e-04	-3.498338e-05
	32×32×3216	0.50	1.008562e-03	-1.253016e-03

References

Blankenbach, B., et al. (1989), A benchmark comparison for mantle convection codes, *Geophys. J. Int.*, *98*, 23–38, doi:10.1111/j.1365-246X.1989.tb05511.x.

King, S. D., C. Lee, P. E. van Keken, W. Leng, S. Zhong, E. Tan, N. Tosi, and M. C. Kameyama (2010), A community benchmark for 2-D Cartesian compressible convection in the Earth's mantle, *Geophysical Journal International*, *180*(1), 73–87, doi:{10.1111/j.1365-246X.2009.04413.x}.

Kramer, S. C., C. R. Wilson, and D. R. Davies (2012), An implicit free surface algorithm for geodynamical simulations, *Physics of the Earth and Planetary Interiors*, *194-195*(0), 25 – 37, doi:10.1016/j.pepi.2012.01.001.

Schubert, G., D. L. Turcotte, and P. Olson (2001), *Mantle Convection in the Earth and Planets*, Cambridge Univ Press.

Simpson, G., and M. Spiegelman (2011), Solitary wave benchmarks in magma dynamics, *J Sci Comput*, doi:10.1007/s10915-011-9461-y.

van Keken, P., et al. (2008), A community benchmark for subduction zone modeling, *Phys. Earth Planet. In.*, *171*(1-4, Sp. Iss. SI), 187–197.

Vatteville, J., P. E. van Keken, A. Limare, and A. Davaille (2009), Starting laminar plumes: Comparison of laboratory and numerical modeling, *Geochem. Geophys. Geosyst.*, *10*, Q12,013, doi:10.1029/2009GC002739.

Zhong, S., M. Gurnis, and L. Moresi (1996), Freesurface formulation of mantle convectionI. Basic theory and application to plumes, *Geophysical Journal International*, *127*(3), 708–718, doi:10.1111/j.1365-246X.1996.tb04049.x.